MICROSCOPY

Ultrastructural characteristics of finger-like membrane protrusions in cell competition

Tomoko Kamasaki[1,2,*], Ryota Uehara[2] and Yasuyuki Fujita[1,3]

[1]Division of Molecular Oncology, Institute for Genetic Medicine, Hokkaido University; Graduate School of Chemical Sciences and Engineering, Hokkaido University, Sapporo, Hokkaido 060-0815, Japan
[2]Faculty of Advanced Life Science, Hokkaido University, Sapporo, Hokkaido 001-0021, Japan
[3]Department of Molecular Oncology, Graduate School of Medicine, Kyoto University, Kyoto 606-8501, Japan
*To whom correspondence should be addressed. E-mail: tkamasaki@igm.hokudai.ac.jp
This manuscript is submitted following a recommendation by the chairperson(s) of the oral session at the 77th Annual Meeting of the Japanese Society of Microscopy.

Abstract

A small number of oncogenic mutated cells sporadically arise within the epithelial monolayer. Newly emerging Ras- or Src-transformed epithelial cells are often apically eliminated during competitive interactions between normal and transformed cells. Our recent electron microscopy (EM) analyses revealed that characteristic finger-like membrane protrusions are formed at the interface between normal and RasV12-transformed cells via the cdc42–formin-binding protein 17 (FBP17) pathway, potentially playing a positive role in intercellular recognition during apical extrusion. However, the spatial distribution and ultrastructural characteristics of finger-like protrusions remain unknown. In this study, we performed both *X–Y* and *X–Z* EM analyses of finger-like protrusions during the apical extrusion of RasV12-transformed cells. Quantification of the distribution and widths of the protrusions showed comparable results between the *X–Y* and *X–Z* sections. Finger-like protrusions were observed throughout the cell boundary between normal and RasV12 cells, except for apicalmost tight junctions. In addition, a non-cell-autonomous reduction in protrusion widths was observed between RasV12 cells and surrounding normal cells under the mix culture condition. In the finger-like protrusions, intercellular adhesions via thin electron-dense plaques were observed, implying that immature and transient forms of desmosomes, adherens junctions or unknown weak adhesions were distributed. Interestingly, unlike RasV12-transformed cells, Src-transformed cells form fewer evident protrusions, and FBP17 in Src cells is dispensable for apical extrusion. Collectively, these results suggest that the dynamic reorganization of intercellular adhesions via finger-like protrusions may positively control cell competition between normal and RasV12-transformed cells. Furthermore, our data indicate a cell context–dependent diversity in the modes of apical extrusion.

Key words: finger-like membrane protrusions, FBP17, cell competition, epithelial cells, Ras, Src

Introduction

Multicellular animals have various mechanisms to avoid damage from stochastic errors or abnormalities occurring within their bodies. In epithelial tissues, normal cells with higher fitness outcompete emerging abnormal cells to maintain homeostasis [1–11]. This homeostatic control mechanism is called cell competition and is broadly conserved among various species from insects [12] to mammals [13]. In an epithelial monolayer, a small population of transformed cells with a mutation in Ras or Src (e.g. RasV12 or SrcY527F) are often apically extruded by surrounding normal cells (apical extrusion [14–17]). This process, termed 'epithelial defense against cancer' (EDAC), potentially serves as an immune system–independent tumor-suppressive mechanism [18]. Although the molecular mechanisms of EDAC are largely unknown, we have identified various factors involved in the competitive interaction between normal and transformed cells. The depletion of E-cadherin in normal cells surrounding transformed cells inhibits apical extrusion [14], suggesting that direct cell–cell adhesion via E-cadherin positively regulates intercellular

recognition between normal and transformed cells. The activity of cdc42 is upregulated within both RasV12-transformed cells and neighboring normal cells only when the transformed cells are surrounded by normal cells [14,19]. Non-cell-autonomous elevation of cdc42 activity is required for the formation of finger-like membrane protrusions at the cell interface and the apical elimination of RasV12 cells [14,19]. These findings suggest that cell–cell contact sites between normal and transformed cells play an essential role in controlling the apical extrusion process. However, the ultrastructural changes in intercellular adhesions that govern apical extrusion are poorly understood.

Using electron microscopy (EM), we recently found that interdigitations of characteristic finger-like membrane protrusions were observed at cell–cell adhesions between RasV12-transformed cells or between normal and RasV12-transformed cells [19]. We also revealed that the formation of finger-like protrusions is mediated by formin-binding protein 17 (FBP17). FBP17 is one of the Bin–Amphiphysin–Rvs (BAR) domain superfamily proteins that bind lipids and deform the

plasma membrane in negative curvature [20,21]. In addition to its direct role in membrane deformation, FBP17 is categorized as a transducer of cdc42-dependent actin assembly proteins essential for Wiskott-Aldrich syndrome protein (WASP)/neural WASP (N-WASP) and Actin-related protein (Arp)2/3 complex–mediated actin nucleation [22,23]. BAR proteins induce the bending of the bound plasma membrane through their intrinsic curvature and thus mediate membrane deformation to form various membrane- and actin-associated structures such as filopodia, lamellipodia, caveolae or endocytic tubules [21,24]. Inhibition of FBP17 or its upstream regulator cdc42 abolishes finger-like protrusions and blocks apical extrusion of RasV12-transformed cells, indicating important contributions of this newly found membrane structure in EDAC [19]. Therefore, FBP17-mediated finger-like protrusions between normal and RasV12-transformed cells may serve as a signaling hub for membrane/cytoskeletal reorganization upon intercellular recognition for apical extrusion. Under EM, the finger-like protrusions in the *X–Y* sections were bent or curved, thinner (∼50 nm) and shorter (∼0.4 μm) structures (Supplementary Fig. S1) [19] compared with filopodia or their precursor microspikes [25–28]. In addition, while highly bundled actin filaments are seen within filopodia or microspikes, a few weak actin filaments run longitudinally within the finger-like protrusions, suggesting that finger-like protrusions have ultrastructural properties distinct from conventional actin-based membrane structures. However, because of the lack of quantitative information from *X–Z* EM analyses of finger-like protrusions, three-dimensional insights into their distribution and ultrastructure are still missing. Moreover, careful quantitative EM analysis is required to understand the spatial relationship between finger-like protrusions and intercellular adhesions, whose physical contributions to apical extrusion have been suggested through functional analyses of E-cadherin [14].

In this study, we demonstrated the ultrastructural characteristics of finger-like membrane protrusions and intercellular adhesions during cell competition through quantitative analyses of both *X–Y* and *X–Z* sections.

Methods
Antibodies and materials
Rat anti-E-cadherin antibody (ECCD-2, 13-1900) and rabbit anti-ZO-1 antibody (61-7300) were from Thermo Fisher Scientific. Alexa Fluor-647-conjugated phalloidin (Invitrogen, Waltham, Massachusetts, USA) was used at 1.0 U/ml. Alexa Fluor-568- and Alexa Fluor-647-conjugated secondary antibodies were from Life Technologies (Waltham, Massachusetts, USA). Rabbit anti-FBP17 antibody [20] was gifted by Dr Toshiki Itoh. Mouse anti-glyceraldehyde-3-phosphate dehydrogenase (GAPDH) antibody (6C5, MAB374) was from Millipore (Darmstadt, Germany). For immunofluorescence, primary antibodies were used at 1:100, and all secondary antibodies were used at 1:200. For western blotting, peroxidase-conjugated anti-rabbit and anti-mouse secondary antibodies were from GE Healthcare (Chicago, Illinois, USA) and Jackson ImmunoResearch (Burlington, Massachusetts, USA), respectively.

Cell culture
Madin–Darby canine kidney (MDCK) cells, MDCK-pTR GFP-RasV12 cells and MDCK-pTR GFP-cSrcY527F cells were cultured as previously described [14,17]. MDCK-pTR GFP-cSrcY527F cells stably expressing canine FBP17-small hairpin (sh)RNA were established similar to a previous study [19]. Briefly, canine FBP17-shRNA template oligonucleotides were cloned into the BglII and XhoI sites of pSUPER.neo+gfp (Oligoengine). Sequences of the oligonucleotides were described previously [19]. MDCK-pTR GFP-cSrcY527F cells were transfected with pSUPER.neo+gfp canine FBP17-shRNA by nucleofection, followed by selection in the medium containing G418.

Immunofluorescence and western blotting
For immunofluorescence, RasV12-transformed cells or cSrc-transformed cells were mixed with non-transformed cells at a ratio of 1:50. The mixture of cells was cultured on coverslips (Matsunami) coated with the collagen matrix as previously described [14,17]. After the cells formed a monolayer, the expression of GFP-RasV12 or GFP-cSrcY527F was induced by tetracycline (Sigma-Aldrich, Burlington, Massachusetts, USA) for 16 h for analyses of non-cell-autonomous changes occurring before apical extrusion or for 24 h for analyses of apical extrusion. Cells were fixed with paraformaldehyde and permeabilized as previously described [14]. Immunofluorescence images were analyzed at 0.5 μm *X–Z* intervals by the FV1000 or FV1200 system (Olympus) equipped with a 60× oil-immersion objective lens (1.35 numerical aperture (NA)). Images were acquired with the Olympus FV10-ASW software. For quantification of apical extrusion of cSrcY527F-transformed cells, one to five transformed cells that were surrounded by normal cells were analyzed. More than 50 colonies of transformed cells were analyzed for each condition, and then the ratio of apical extrusion of transformed cells was quantified. Western blotting was performed as previously described [29]. Primary antibodies were used at 1:500 or 1:2000 for anti-FBP17 antibody or anti-GAPDH antibody, respectively. Western blotting data were analyzed using LuminoGraph WSE-6100 (ATTO).

Electron microscopy
EM analyses were performed as previously described [15,19]. Briefly, cells were cultured in collagen gel–coated, grid-imprinted plastic dishes (μ-Dish 35-mm Grid-500, ibidi, Gräfelfing, Germany). Cells were fixed with 2% glutaraldehyde (Electron Microscopy Sciences, Hatfield, Pennsylvania, USA) in 4-(2-hydroxyethyl)-1-piperazineethanesulfonic acid (HEPES) buffer (pH 7.4; 30-mM HEPES, 0.1 M NaCl and 2 mM CaCl$_2$). Fluorescence and differential interference contrast (DIC) images of GFP-RasV12 cells and surrounding normal cells were recorded, together with the underlying grid information. Cells were fixed and stained with 2% osmium tetroxide in 0.1 M imidazole (pH 7.4) and 1% uranyl acetate. After dehydration and substitution, the cells were embedded in epoxy resin. Resin-embedded samples were then removed from plastic dishes. At this point, the grid pattern was transferred to the surface of the sample. For *X–Z* analyses of the mix culture of normal and GFP-RasV12 cells, a shallow line of a razor blade was first carved into a layer of collagen gel above the second row of normal cells surrounding RasV12 cells (Fig. 1 (1), blue arrow). The knife mark served as a landmark to determine the region of interest (ROI) during EM observation. The first row of normal cells surrounding RasV12 cells was roughly exposed by fracturing along the

X–Z plane with a razor blade (Fig. 1, (2), red line). In this process, the fractured *X–Z* surface should be roughly perpendicular to the knife mark, which was carved in step (1). After the sample was mounted on a base such that the fractured surface was oriented upward, trimming and sectioning were performed (Fig. 1, (3) and (4)). To easily find the ROI, the location of the knife mark carved in step (1) in a trimmed sample should be roughly noted (Fig. 1, (4), e.g. 1/3 from the left side of the sample). Ultrathin sections (~70 nm) were mounted on formvar-coated copper grids (SP 3 slit mesh; Nisshin EM, Tokyo, Japan), and the samples were imaged using a transmission electron microscope (JEM-1400, JEOL, Tokyo, Japan) operating at 80 kV (Fig. 1, (5)). EM images were analyzed using the 3DMOD program [30]. Briefly, cell membranes at cell–cell contact sites were manually traced using EM images originally taken at ~6000×. The lengths of the cell membranes and cell boundaries were measured to calculate the waviness of the cell membranes. The number and width of the finger-like protrusions were similarly counted and measured using the 3DMOD program.

Quantification and statistical analysis

For statistical analyses, unpaired two-tailed Student's *t*-tests were used to determine *P*-values. *P*-values <0.05 were considered to be significant. No statistical method was used to predetermine sample size.

The numbers of the analyzed samples in each figure are as follows. All data were obtained from three independent experiments. For Fig. 2c and d, 6, 6, 6, 6 and 10 boundaries for waviness of cell membranes (c; left to right in the graph) and 7, 10, 6, 6 and 10 boundaries for frequency of protrusions (d; left to right in the graph) were analyzed. For Fig. 3, 66 (MDCK), 154 (RasV12), 158 (MDCK side at MDCK-RasV12), 153 (RasV12 side at MDCK-RasV12) and 223 (RasV12-RasV12 surrounded by MDCK) protrusions were analyzed. For Fig. 4d and Supplementary Fig. 4b, 45, 16, 55 and 19 cell adhesions (left to right in the panel) were analyzed. For Fig. 5b, 20, 13 and 34 boundaries (left to right in the graph) were analyzed. For Fig. 5e, 117, 116 and 108 cells for cSrcY527F; 84, 84 and 80 cells for cSrcY527F FBP17-shRNA1; and 93, 85 and 88 cells for cSrcY527F FBP17-shRNA2 were analyzed. For Supplementary Fig. 2a, 66 (MDCK), 154 (RasV12), 158 (MDCK side at MDCK-RasV12), 153 (RasV12 side at MDCK-RasV12) and 223 (RasV12-RasV12 surrounded by MDCK) protrusions were analyzed. For Supplementary Fig. 2b, 18 (MDCK), 84 (RasV12), 47 (MDCK side at MDCK-RasV12), 37 (RasV12 side at MDCK-RasV12) and 72 (RasV12-RasV12 surrounded by MDCK) protrusions were analyzed. For Supplementary Fig. 3, 18 (MDCK), 84 (RasV12), 47 (MDCK side at MDCK-RasV12), 37 (RasV12 side at MDCK-RasV12) and 72 (RasV12-RasV12 surrounded by MDCK) protrusions were analyzed. For Supplementary Fig. 4c, 14 (MDCK), 10 (RasV12), 32 (MDCK-RasV12) and 15 (RasV12-RasV12 surrounded by MDCK) cell adhesions were analyzed.

Results

Formation of finger-like membrane protrusions between normal and RasV12-transformed epithelial cells or between RasV12 cells in *X-Z* sections

We previously performed ultrastructural analyses of intercellular adhesion sites in alone or mix cultures of normal and RasV12-transformed MDCK cells using *X–Y* sections [19]. These observations demonstrated that finger-like membrane protrusions (Supplementary Fig. S1) are formed more frequently in RasV12 cells than in normal cells under the alone culture conditions. In contrast, in mix culture, finger-like protrusions are non-cell-autonomously promoted in normal cells toward neighboring RasV12 cells as well as between RasV12 cells. To gain insights into the 3-dimensional ultrastructural organization of the interfaces among these cells, we analyzed cell membranes of intercellular adhesion sites using correlative light and EM of *X–Z* sections (Fig. 1, see details in the 'Electron microscopy' section; Fig. 2). In alone cultures or in a mix culture of normal and RasV12-transformed cells, finger-like protrusions appeared throughout cell–cell adhesions, except for apicalmost tight junction regions (Fig. 2a). In the alone culture of normal cells, the cell membranes of the intercellular region intermittently formed finger-like protrusions (Fig. 2a, left panels). In contrast, in the alone culture of RasV12 cells, the cell membranes were wavier with a significant increase in finger-like protrusions (Fig. 2a, middle panels). At the interface between normal and RasV12 cells or between RasV12 cells in the mix culture, finger-like protrusions were observed on both sides of the cells (Fig. 2a, right panels). To quantify the characteristics of the intercellular regions in the *X–Z* sections, we set two indices: waviness of cell membranes and frequency of protrusions (Fig. 2b). Both cell membrane waviness and protrusion frequency were significantly higher in RasV12 cells than those in normal cells under alone culture conditions (Fig. 2c and d). In the mix culture, compared to the alone culture, both indices increased on the side of normal MDCK cells at the MDCK-RasV12 boundary or the interfaces between RasV12 cells surrounded by normal cells (Fig. 2c and d). Therefore, MDCK-RasV12 cell interfaces in the *X–Z* sections showed complex membrane reorganization comparable to that observed in the *X–Y* sections [19].

Non-cell-autonomous changes in width distribution of the finger-like protrusions in the mix culture of normal and RasV12 cells

In the course of the EM observations, we noticed a substantial variety in the widths of the finger-like protrusions. To gain insight into the protrusion width distribution, we compared the inner widths of individual protrusions at the cell boundaries in the *X–Y* and *X–Z* sections in alone or mix cultures (Supplementary Fig. S2). While >60% of the protrusions had a width <60 nm with a relatively sharp peak in the range of 40–60 nm in the alone culture of RasV12 cells, the normal MDCK cells in the alone culture tended to have wider protrusions with less prominent peaks (Fig. 3a; Supplementary Figs. S2 and S3a). Interestingly, however, under the mix culture condition, protrusions in the normal MDCK cells at the MDCK-RasV12 boundary became thinner than those in the MDCK alone culture, with a sharp peak in the 40–60-nm range (Fig. 3b; Supplementary Figs. S2 and S3b). Similarly, protrusions were likely to be thinner at the interfaces among RasV12 cells surrounded by normal cells, with a drastic increase in a population of 20–40-nm-wide protrusions compared to those in the RasV12 alone culture (Fig. 3c; Supplementary Figs. S2 and S3c). These data demonstrate a non-cell-autonomous change in the ultrastructural features of finger-like protrusions in the mix culture of normal and RasV12-transformed cells.
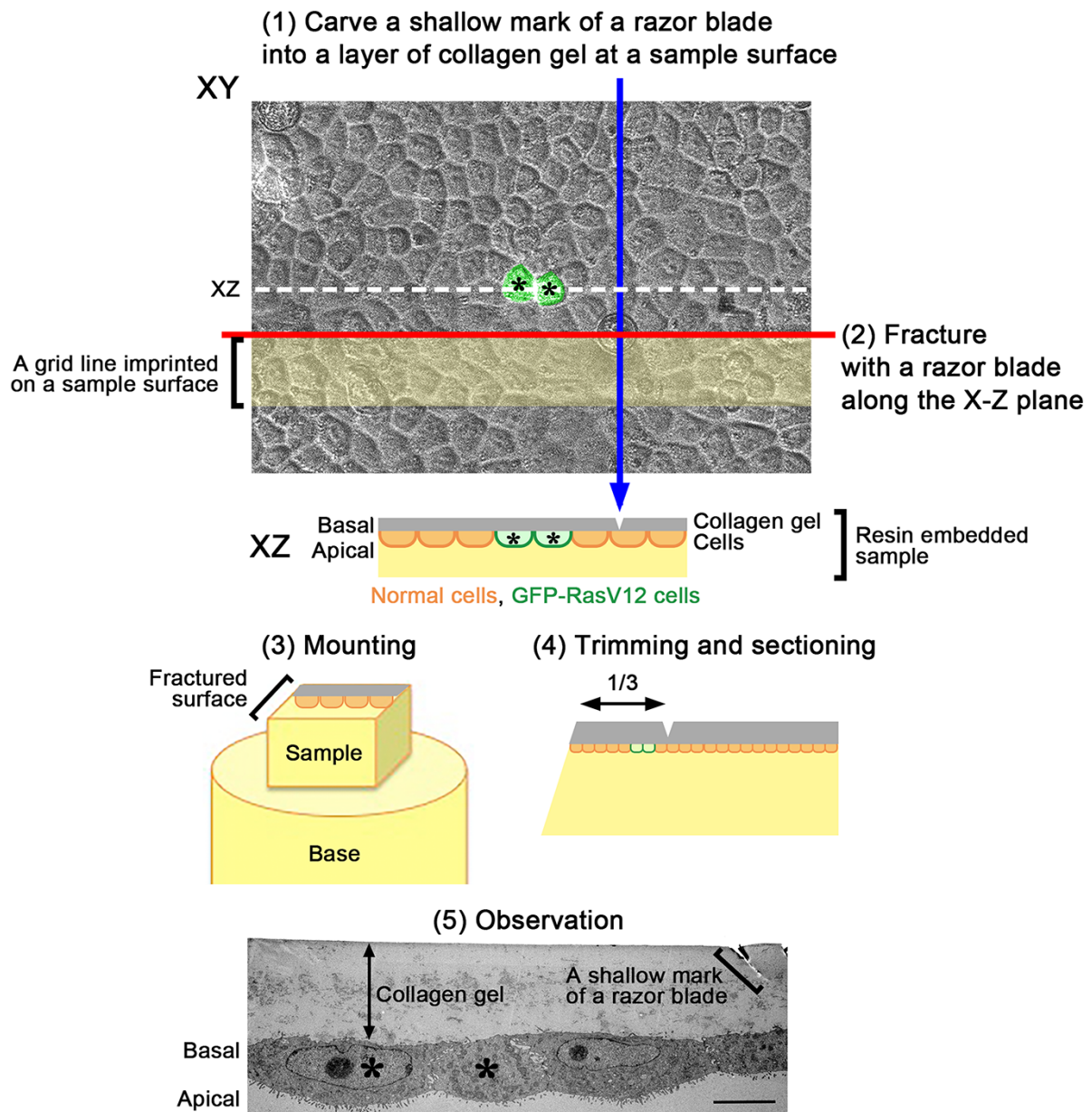
Fig. 1. A schematic diagram of a procedure for analyzing the mix culture of normal and transformed cells using *X–Z* sections. A light microscopic image shown on the upper side represents GFP-RasV12 cells and surrounding normal cells that were cultured in collagen gel–coated, grid-imprinted plastic dishes. GFP-RasV12 cells are represented in asterisks. Scale bar, 5 μm (lower panel). See the details in the 'Electron microscopy' section.

Cell adhesions within the finger-like protrusions

E-cadherin-based intercellular adhesion of normal cells surrounding RasV12-transformed cells plays an important role in the apical extrusion of RasV12 cells from a monolayer of epithelial cells [14]. To gain insights into the spatial relationship between the finger-like protrusions and cell–cell adhesion structures under EM, we first observed the localization of E-cadherin (a component of adherens junctions and nascent desmosomes [31,32]) and ZO-1 (a component of tight junctions [33]) using immunofluorescence (Fig. 4a). While these proteins accumulated ubiquitously at cell–cell adhesion sites in alone or mix cultures of normal and RasV12 cells (Fig. 4a), we often observed more intense and thicker signals of E-cadherin or GFP-RasV12 (the cell membrane protein) at the interfaces between RasV12 cells surrounded

by normal cells during apical extrusion (Fig. 4a, right panels). The broadening of E-cadherin and GFP-RasV12 signals possibly reflected the formation of deeper interdigitations of finger-like protrusions at the interface between RasV12 cells surrounded by normal cells (Fig. 2a, c and d [19]). We then analyzed the ultrastructures of intercellular adhesions and their arrangements in the alone or mix culture with *X–Y* sections. Under EM, intercellular adhesions such as desmosomes and adherens junctions appear as thick or thin electron-dense plaques of closely apposed cell membranes between cells (Fig. 4b [31,34]). Cell adhesion via thick plaques associated with intermediate filaments is categorized as mature desmosomes [34,35]. In contrast, cell adhesion via thin plaques is classified as immature and transient forms of desmosomes, adherens junctions or other unidentified weak
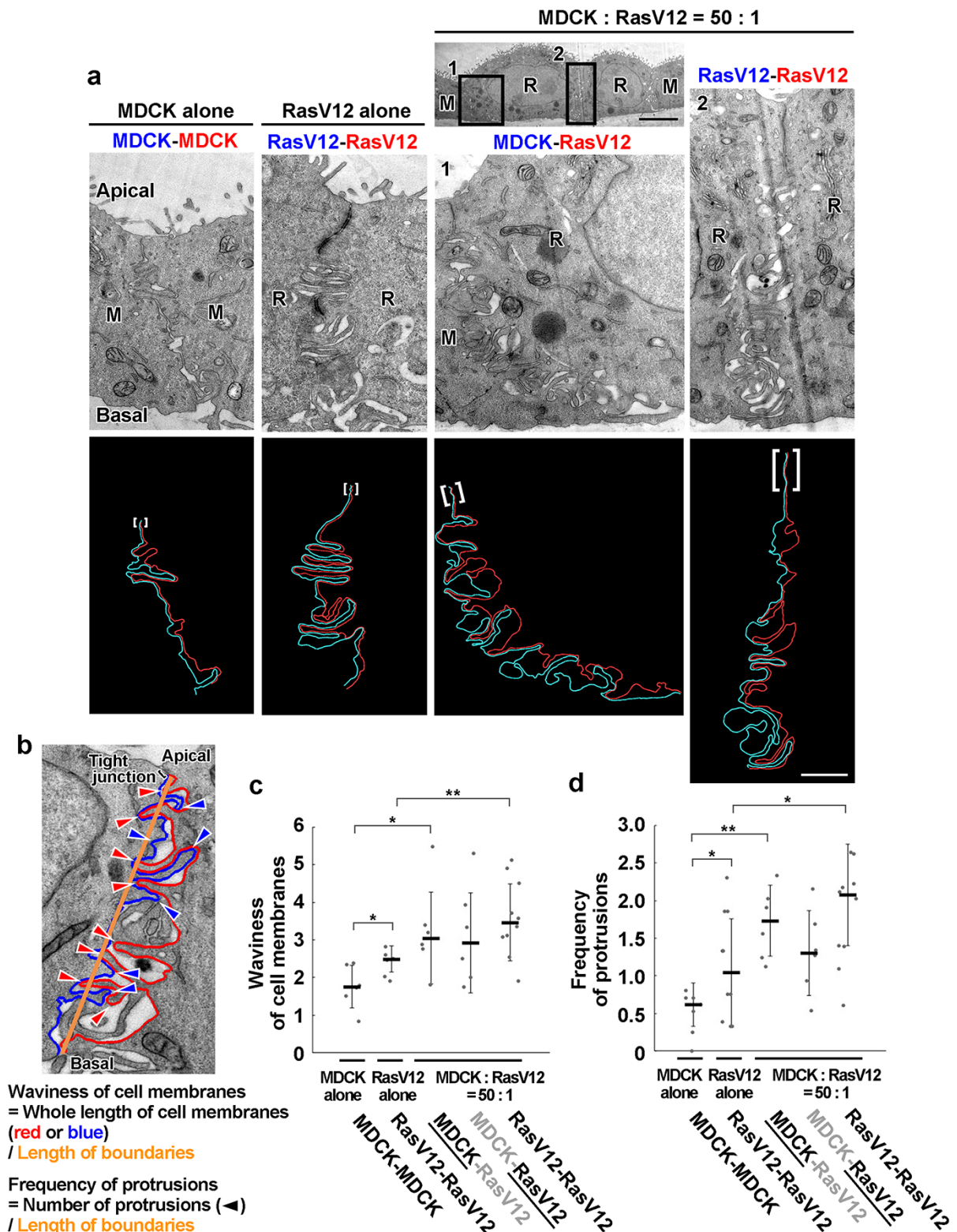
Fig. 2. The formation of finger-like membrane protrusions is promoted in RasV12-transformed cells and the neighboring normal cells also in *X-Z* sections. (a) EM images showing the alone or mix cultures of normal and RasV12-transformed MDCK cells. Cells were fixed at 16 h after the induction of RasV12 and sectioned along the *X–Z* axis. The areas in the black boxes in an upper panel are shown in right panels at higher magnification, representing intercellular regions. Tracings of cell membranes at cell–cell contacts are demonstrated in lower panels. Brackets represent the tight junction areas. Scale bars of 5 µm (upper panel) and 1 µm (middle and lower panels). (b) An example for analyses of the waviness of cell membranes and the frequency of protrusions. A protrusive plasma membrane of which length is longer than the width is defined as 'protrusion'. The cell boundary is defined as a line connecting both apical and basal edges of cell membranes except the tight junction area. (c, d) Waviness of cell membranes (c) or frequency of protrusions (d) at each cell–cell contact in the alone or mix culture. As for the MDCK-RasV12 boundary, the data on the underlined side are shown. Data are median ± SD. *$P < 0.05$, **$P < 0.01$ (unpaired two-tailed Student's *t*-tests).

a

MDCK alone, MDCK-MDCK
RasV12 alone, RasV12-RasV12

b

MDCK alone, MDCK-MDCK
MDCK : RasV12 = 50 : 1, MDCK-RasV12

c

RasV12 alone, RasV12-RasV12
MDCK : RasV12 = 50 : 1, RasV12-RasV12
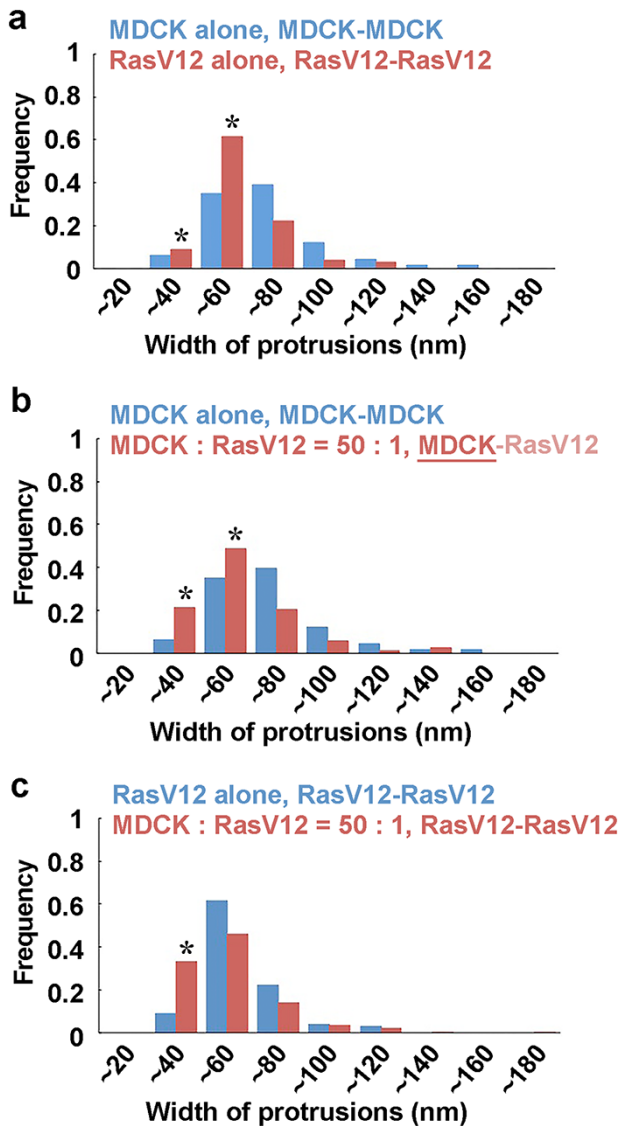
Fig. 3. Width distribution of the finger-like membrane protrusions after cell-autonomous or non-cell-autonomous changes. For measurements of widths of protrusions, a part of the protrusion whose width is constant over 50 nm was selected near the cell body. Inner widths of finger-like protrusions in *X–Y* sections were measured. Positions of the cell boundaries plotted in each histogram are shown on the upper side. Asterisks represent ranges that have higher frequency after cell-autonomous (a) or non-cell-autonomous (b, c) changes.

adhesions. Under the alone or mix culture conditions, cell adhesions via thick plaques were usually observed in smooth cell membranes, except for finger-like protrusions, while cell adhesions via thin plaques were observed between cell bodies, between a cell body and a protrusion or between protrusions (Fig. 4c). In addition, cell adhesion via thin plaques within the finger-like protrusions appeared to be randomly distributed. We then analyzed the frequency of cell adhesion via thin plaques at each category of cell interface in the alone or mix culture (Fig. 4d). Under the MDCK alone culture condition, cell adhesions via thin plaques were most frequently formed between cell bodies (Fig. 4d, left graph). On the other hand, in the RasV12 alone culture as well as the mix culture of normal and RasV12 cells, cell adhesions via thin plaques were

also formed between the cell body and a protrusion at an equivalent or higher frequency as those between cell bodies (Fig. 4d, right three graphs). Cell adhesion via thin plaques at the protrusion-protrusion interfaces also increased under these conditions. In most cases, the long axis of the finger-like protrusions was oriented approximately perpendicular to the cell boundary (Supplementary Fig. S1; Fig. 2). Consistent with this result, cell adhesion via thin plaques within protrusions tended to be angled against the cell boundary (Supplementary Fig. S4a and b). These results suggest that cell adhesion via thin plaques is maintained or formed even at cell–cell contact sites predominantly occupied by the finger-like protrusions.

FBP17 in cSrcY527F-transformed cells does not play an important role in apical extrusion

Previous studies have revealed several molecules commonly involved in the apical extrusion of RasV12- or Src-transformed cells [14–18]. Our previous EM analysis demonstrated that FBP17-mediated finger-like membrane protrusions in RasV12 cells induced apical elimination in intercellular regions [19]. To test the contributions of FBP17-dependent membrane/cytoskeletal reorganization in cells with the other oncogenic mutation, we investigated the ultra-structures of cell–cell contact sites and the effects of FBP17 depletion in cSrcY527F cells (Fig. 5). Under the alone culture condition, RasV12 cells had numerous finger-like protrusions at the intercellular regions compared to normal MDCK cells (Fig. 5a, left and middle panels). In contrast, in cSrcY527F cells, cell–cell contact sites were flat and smooth with short protrusions (Fig. 5a, right panels). Consistent with these observations, the waviness of the cell membrane of cSrcY527F cells was significantly lower than that of RasV12 cells (Fig. 5b). Next, we examined the fate of FBP17-knockdown cSrcY527 cells surrounded by normal cells in a mix culture (Fig. 5c–e). We found that FBP17 depletion in cSrcY527F cells did not affect the apical extrusion ratio (Fig. 5d and e). These results imply that intercellular recognition between normal and Src-transformed cells may be induced independently of FBP17-mediated finger-like protrusions during cell competition.

Discussion

Our EM analyses using both *X–Y* and *X–Z* sections revealed the ultrastructural characteristics of the reorganization of cell interfaces during cell competition between normal and RasV12-transformed cells. The trends of membrane waviness and formation of finger-like protrusion in the *X–Z* sections are comparable to those in the *X–Y* sections [19]. Moreover, width distributions of the finger-like protrusions are similar between the *X–Y* and *X–Z* sections, suggesting a cylindrical shape of the protrusions. When RasV12-transformed cells are surrounded by normal cells, the formation of finger-like protrusions is promoted, with an evident reduction in their width in both normal and surrounded RasV12-transformed cells. These results highlight a non-cell-autonomous ultra-structural reorganization at the cell interface during cell competition. Moreover, these data imply that finger-like protrusion-mediated intercellular recognition between nor-mal and transformed cells [19] may evenly occur throughout
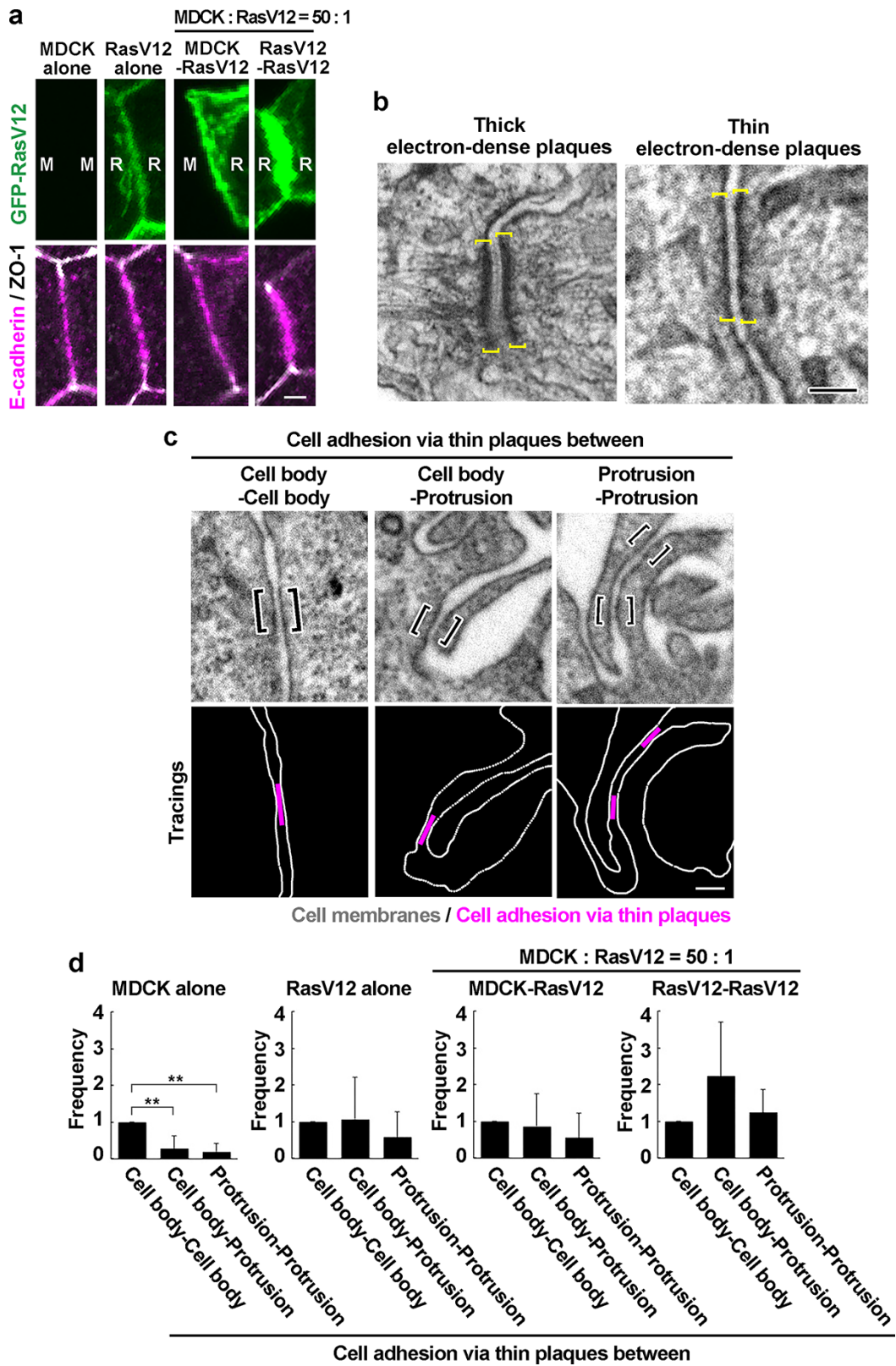
Fig. 4. Ultrastructure of cell adhesions within finger-like protrusions. Data were obtained from the $X-Y$ sections. (a) Immunofluorescence images of cell boundaries in alone or mix cultures of normal and RasV12-transformed cells. Scale bar of 10 μm. (b) Cell adhesions via thick or thin electron-dense plaques. In this study, thick or thin plaques were categorized by a ratio of thickness against cell membranes (thick: ∼2.6; thin: ∼1.2). Brackets represent electron-dense plaques along cell membranes. (c) EM images and tracings of cell adhesion via thin plaques that were observed between cell bodies (left), between the cell body and protrusion (middle) and between protrusions (right). Brackets represent the position of cell adhesion via thin plaques. Scale bars of 0.1 μm (b, c). (d) Frequency of cell adhesion via thin plaques observed in each category in the alone or mix culture. A ratio of the frequency (number of the cell adhesions/length of cell boundaries) relative to cell body–cell body was plotted. $**P < 0.01$ (unpaired two-tailed Student's t-tests).
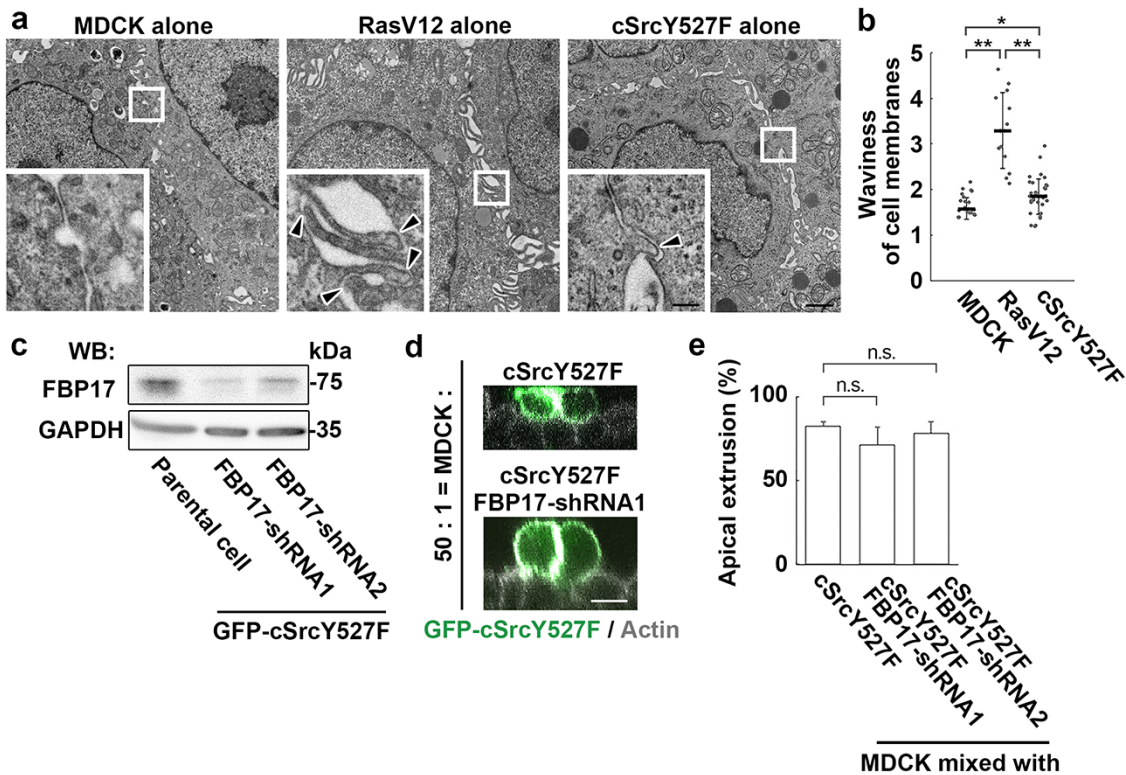
Fig. 5. FBP17 in cSrcY527F-transformed cells is dispensable for apical extrusion. (a) EM images of normal MDCK cells, RasV12-transformed cells or cSrcY527F-transformed cells under alone culture conditions. X–Y sections. The areas in the white boxes are shown as insets at higher magnification, demonstrating intercellular regions. Arrowheads represent finger-like protrusions. Scale bars of 1 and 0.2 μm (insets). (b) Quantification of the waviness of cell membranes. Data are median ± SD. *$P < 0.05$, **$P < 0.01$ (unpaired two-tailed Student's t-tests). (c) Establishment of MDCK-pTR GFP-cSrcY527F cells stably expressing FBP17-shRNA1 or 2. Cell lysates were analyzed by western blotting with the indicated antibodies. (d) X–Z fluorescence images of cSrcY527F cells or FBP17-knockdown cSrcY527F cells surrounded by normal cells. Scale bar of 10 μm. (e) Effect of FBP17 knockdown in cSrcY527F-transformed cells on apical extrusion.

cell–cell contact sites, except for tight junctions in both the X–Y and X–Z dimensions.

We previously showed that the formation of finger-like protrusions at cell interfaces is mediated by FBP17 [19]. Under the alone culture condition, FBP17 is cell-autonomously accumulated at the cell–cell contact sites of RasV12 cells. In the mix culture of normal and RasV12 cells, FBP17 is non-cell-autonomously concentrated at the lateral side of the cell membranes in normal MDCK cells around RasV12 cells and between RasV12 cells surrounded by normal cells. FBP17 plays a role in the formation of cell membranes with negative curvatures, such as endocytic invaginations/tubules and caveolae. Additionally, FBP17 is thought to deform cell membranes in a dose-dependent manner as an N-WASP activator, inducing actin polymerization via activation of the Arp2/3 complex [20,36]. Our previous immuno-EM analyses have shown that FBP17 seems to accumulate more frequently at the base of finger-like protrusions than on the lateral sides [19]. Therefore, the non-cell-autonomous reduction in the width of protrusions might be controlled by invagination formation and membrane internalization at the base of the finger-like protrusions via FBP17, which accumulates at the cell boundaries under the mix culture condition (Fig. 6, left).

Our EM analyses also revealed that cell adhesions via thin electron-dense plaques exist not only between cell bodies but also between a cell body and a protrusion or between protrusions in both alone and mix cultures (Fig. 6, left). Cell
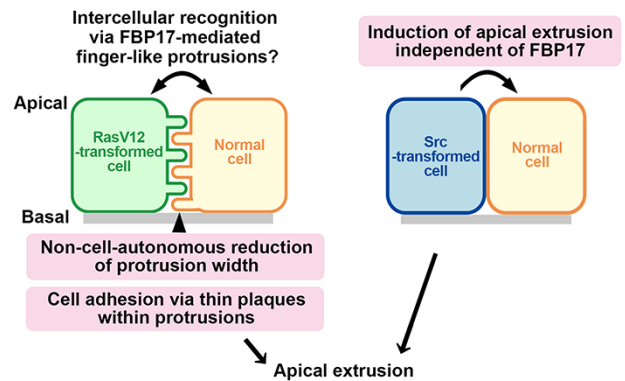
Fig. 6. Schematic diagrams for intercellular recognition at the boundary between normal and transformed cells.

adhesion via thin plaques potentially corresponds to immature and transient forms of desmosomes, adherens junctions or unidentified weak adhesions. In future studies, immuno-EM and/or super-resolution microscopic analyses will be needed to categorize these intercellular adhesion structures and gain insights into their distributions. It has been reported that one type of nascent adherens junction between protrusions at the intercellular region is called 'punctum adherens' [35,37–40]. The length of the cell adhesion via thin plaques observed in this study (Supplementary Fig. S4c) was similar

to that of punctum adherens (100–150 nm length). However, the length and width of the finger-like protrusions are much shorter (∼0.4 μm) and thinner (∼50 nm), respectively, than those of the protrusions involved in the punctum adherens. Interestingly, at the boundary between normal and RasV12-transformed cells, the length of cell adhesion via thin plaques tends to have larger deviations compared to that of alone cultures or RasV12 cells surrounded by normal cells (Supplementary Fig. S4c), implying irregular or asynchronous dynamics of finger-like protrusions between the normal and RasV12-transformed cells during competitive interactions.

Cell–cell adhesion is the site where cells experience tugging forces. Previous studies have proposed that cadherin adhesion molecules may serve as mechanotransducers at cell–cell contacts [41,42]. Therefore, alterations in the orientation of cell adhesions via thin plaques upon the formation of finger-like protrusions potentially change the mode of mechanotransduction at the boundary between normal and RasV12-transformed cells, which may impact the process of apical extrusion. It has been demonstrated that FBP17 tends to accumulate at cell membranes where tension increases, such as at the leading edge of motile cells or apical membranes forced by high osmotic pressure [43,44]. Indeed, our recent fluorescent microscopy analysis using a membrane tension sensor showed that membrane tension tends to increase at the boundary between normal and RasV12 cells (Kuromiya *et al.* in revision), implying a link between FBP17-dependent ultrastructural changes and mechanical alterations at the cell interfaces during the induction of apical extrusion. In future studies, the upstream mechanism of the intercellular recognition machinery between normal and transformed cells via finger-like protrusions should be clarified.

What is the possible function of FBP17-mediated finger-like protrusions in normal cells surrounding RasV12-transformed cells for apical extrusion after intercellular recognition? Before apical extrusion starts, transient upsurges of intracellular calcium named 'calcium wave', regulated by endoplasmic reticulum protein IP3 receptor, gap junction and mechanosensitive calcium channel short transient receptor potential channel 1 (TRPC1), propagate from transformed cells within the epithelium [45]. Calcium wave promotes apical extrusion of transformed cells through the induction of polarized movement of surrounding normal cells toward extruding cells. Our previous study demonstrated that cdc42 activity is non-cell-autonomously elevated in normal cells around RasV12 cells, leading to FBP17-mediated finger-like protrusions [19]. Such calcium waves and the upregulation of cdc42 activity do not occur in the alone cultures of normal or RasV12 cells, demonstrating the importance of these mechanisms for EDAC. Moreover, another study has shown a correlation between the oscillation of intercellular calcium and the cdc42–FBP17 pathway [46]. In future studies, the possibility of whether or how cdc42–FBP17–mediated finger-like protrusions trigger calcium waves to propagate the directed cell migration of surrounding normal cells for apical extrusion at both molecular and mechanical levels will be examined.

In contrast to RasV12-transformed cells, finger-like protrusions are much less evident in cSrcY527F cells under the alone culture condition. Consistent with this observation, FBP17 in cSrcY527F cells is dispensable for apical extrusion (Fig. 6, right). Therefore, any mechanism independent of FBP17-mediated finger-like protrusions would govern apical

extrusion of Src-transformed cells, implying cell context–dependent diversity in modes of cell–cell interface reorganization for cell competition. Further studies are required to clarify how the ultrastructural differences between RasV12- and Src-transformed cells are linked to the dynamics and molecular requirements of their apical extrusion processes.

Concluding remarks

We have demonstrated the detailed ultrastructural features of cell interfaces, which dynamically change in a non-cell-autonomous manner and potentially impact the physical and mechanical properties of cell–cell interactions during apical extrusion. A comparison between cells with different mutational backgrounds revealed diversity in the regulatory mechanisms of apical extrusion at both ultrastructural and molecular levels. Further investigations on the control of cell–cell interactions in different cell backgrounds are required for a comprehensive understanding of the processes of EDAC.

Supplementary data

Supplementary data are available at *Microscopy* online.

Conflict of interest

The authors declare that they have no conflict of interest.

References

1. Amoyel M and Bach E A (2014) Cell competition: how to eliminate your neighbours. *Development* 141: 988–1000.
2. Baker N E (2011) Cell competition. *Curr. Biol.* 21: R11–R15.
3. Bowling S, Lawlor K, and Rodriguez T A (2019) Cell competition: the winners and losers of fitness selection. *Development* 146: dev167486.

4. Claveria C and Torres M (2016) Cell competition: mechanisms and physiological roles. *Annu. Rev. Cell Dev. Biol.* 32: 411–439.

5. Johnston L A (2009) Competitive interactions between cells: death, growth, and geography. *Science* 324: 1679–1682.

6. Levayer R (2020) Solid stress, competition for space and cancer: the opposing roles of mechanical cell competition in tumour initiation and growth. *Semin. Cancer Biol.* 63: 69–80.

7. Merino M M, Levayer R, and Moreno E (2016) Survival of the fittest: essential roles of cell competition in development, aging, and cancer. *Trends. Cell Biol.* 26: 776–788.

8. Morata G and Calleja M (2020) Cell competition and tumorigenesis in the imaginal discs of *Drosophila*. *Semin. Cancer Biol.* 63: 19–26.

9. Ohsawa S, Vaughen J, and Igaki T (2018) Cell extrusion: a stress-responsive force for good or evil in epithelial homeostasis. *Dev. Cell* 44: 532.

10. Vincent J P, Fletcher A G, and Baena-Lopez L A (2013) Mechanisms and mechanics of cell competition in epithelia. *Nat. Rev. Mol. Cell Biol.* 14: 581–591.

11. Wagstaff L, Kolahgar G, and Piddini E (2013) Competitive cell interactions in cancer: a cellular tug of war. *Trends Cell Biol.* 23: 160–167.

12. Morata G and Ripoll P (1975) Minutes: mutants of drosophila autonomously affecting cell division rate. *Dev. Biol.* 42: 211–221.

13. Kon S and Fujita Y (2021) Cell competition-induced apical elimination of transformed cells, EDAC, orchestrates the cellular homeostasis. *Dev. Biol.* 476: 112–116.

14. Hogan C, Dupre-Crochet S, Norman M, Kajita M, Zimmermann C, Pelling A E, Piddini E, Baena-Lopez L A, Vincent J P, Itoh Y, and Hosoya H (2009) Characterization of the interface between normal and transformed epithelial cells. *Nat. Cell Biol.* 11: 460–467.

15. Kon S, Ishibashi K, Katoh H, Kitamoto S, Shirai T, Tanaka S, Kajita M, Ishikawa S, Yamauchi H, Yako Y, and Kamasaki T (2017) Cell competition with normal epithelial cells promotes apical extrusion of transformed cells through metabolic changes. *Nat. Cell Biol.* 19: 530–541.

16. Kajita M, Hogan C, Harris A R, Dupre-Crochet S, Itasaki N, Kawakami K, Charras G, Tada M, and Fujita Y (2010) Interaction with surrounding normal epithelial cells influences signalling pathways and behaviour of Src-transformed cells. *J. Cell Sci.* 123: 171–180.

17. Ohoka A, Kajita M, Ikenouchi J, Yako Y, Kitamoto S, Kon S, Ikegawa M, Shimada T, Ishikawa S, and Fujita Y (2015) EPLIN is a crucial regulator for extrusion of RasV12-transformed cells. *J. Cell Sci.* 128: 781–789.

18. Kajita M, Sugimura K, Ohoka A, Burden J, Suganuma H, Ikegawa M, Shimada T, Kitamura T, Shindoh M, Ishikawa S, and Yamamoto S (2014) Filamin acts as a key regulator in epithelial defence against transformed cells. *Nat. Commun.* 5: 4428.

19. Kamasaki T, Miyazaki Y, Ishikawa S, Hoshiba K, Kuromiya K, Tanimura N, Mori Y, Tsutsumi M, Nemoto T, Uehara R, and Suetsugu S (2021) FBP17-mediated finger-like membrane protrusions in cell competition between normal and RasV12-transformed cells. *iScience* 24: 102994.

20. Itoh T, Erdmann K S, Roux A, Habermann B, Werner H, and De Camilli P (2005) Dynamin and the actin cytoskeleton cooperatively regulate plasma membrane invagination by BAR and F-BAR proteins. *Dev. Cell* 9: 791–804.

21. Suetsugu S, Kurisu S, and Takenawa T (2014) Dynamic shaping of cellular membranes by phospholipids and membrane-deforming proteins. *Physiol. Rev.* 94: 1219–1248.

22. Ho H Y, Rohatgi R, Lebensohn A M, Le M, Li J, Gygi S P, and Kirschner M W (2004) Toca-1 mediates Cdc42-dependent actin nucleation by activating the N-WASP-WIP complex. *Cell* 118: 203–216.

23. Takenawa T and Suetsugu S (2007) The WASP-WAVE protein network: connecting the membrane to the cytoskeleton. *Nat. Rev. Mol. Cell Biol.* 8: 37–48.

24. Frost A, Unger V M, and De Camilli P (2009) The BAR domain superfamily: membrane-molding macromolecules. *Cell* 137: 191–196.

25. Mattila P K and Lappalainen P (2008) Filopodia: molecular architecture and cellular functions. *Nat. Rev. Mol. Cell Biol.* 9: 446–454.

26. Vasioukhin V, Bauer C, Yin M, and Fuchs E (2000) Directed actin polymerization is the driving force for epithelial cell-cell adhesion. *Cell* 100: 209–219.

27. Welch M D and Mullins R D (2002) Cellular control of actin nucleation. *Annu. Rev. Cell Dev. Biol.* 18: 247–288.

28. Svitkina T M, Bulanova E A, Chaga O Y, Vignjevic D M, Kojima S, Vasiliev J M, and Borisy G (2003) Mechanism of filopodia initiation by reorganization of a dendritic network. *J. Cell Biol.* 160: 409–421.

29. Hogan C, Serpente N, Cogram P, Hosking C R, Bialucha C U, Feller S M, Braga V M, Birchmeier W, and Fujita Y (2004) Rap1 regulates the formation of E-cadherin-based cell-cell contacts. *Mol. Cell Biol.* 24: 6690–6700.

30. Kremer J R, Mastronarde D N, and McIntosh J R (1996) Computer visualization of three-dimensional image data using IMOD. *J. Struct. Biol.* 116: 71–76.

31. Takeichi M (1988) The cadherins: cell-cell adhesion molecules controlling animal morphogenesis. *Development* 102: 639–655.

32. Shafraz O, Rubsam M, Stahley S N, Caldara A L, Kowalczyk A P, Niessen C M, and Sivasankar S (2018) E-cadherin binds to desmoglein to facilitate desmosome assembly. *eLlife* 7: e37629.

33. Furuse M, Itoh M, Hirase T, Nagafuchi A, Yonemura S, Tsukita S, and Tsukita S (1994) Direct association of occludin with ZO-1 and its possible involvement in the localization of occludin at tight junctions. *J. Cell Biol.* 127: 1617–1626.

34. Perez-Moreno M, Jamora C, and Fuchs E (2003) Sticky business: orchestrating cellular signals at adherens junctions. *Cell* 112: 535–548.

35. Yonemura S, Itoh M, Nagafuchi A, and Tsukita S (1995) Cell-to-cell adherens junction formation and actin filament organization: similarities and differences between non-polarized fibroblasts and polarized epithelial cells. *J. Cell Sci.* 108: 127–142.

36. Tsujita K, Suetsugu S, Sasaki N, Furutani M, Oikawa T, and Takenawa T (2006) Coordination between the actin cytoskeleton and membrane deformation by a novel membrane tubulation domain of PCH proteins is involved in endocytosis. *J. Cell Biol.* 172: 269–279.

37. Farquhar M G and Palade G E (1963) Junctional complexes in various epithelia. *J. Cell Biol.* 17: 375–412.

38. Tepass U and Hartenstein V (1994) The development of cellular junctions in the Drosophila embryo. *Dev. Biol.* 161: 563–596.

39. Rose O, Grund C, Reinhardt S, Starzinski-Powitz A, and Franke W (1995) Contactus adherens, a special type of plaque-bearing adhering junction containing M-cadherin, in the granule cell layer of the cerebellar glomerulus. *Proc. Natl. Acad. Sci. U. S. A.* 92: 6022–6026.

40. Yonemura S (2011) Cadherin-actin interactions at adherens junctions. *Curr. Opin. Cell Biol.* 23: 515–522.

41. Yonemura S, Wada Y, Watanabe T, Nagafuchi A, and Shibata M (2010) alpha-Catenin as a tension transducer that induces adherens junction development. *Nat. Cell Biol.* 12: 533–542.

42. Charras G and Yap A S (2018) Tensile forces and mechanotransduction at cell-cell junctions. *Curr. Biol.* 28: R445–R457.

43. Tsujita K, Takenawa T, and Itoh T (2015) Feedback regulation between plasma membrane tension and membrane-bending

proteins organizes cell polarity during leading edge formation. *Nat. Cell Biol.* 17: 749–758.

44. Echarri A, Pavon D M, Sanchez S, Garcia-Garcia M, Calvo E, Huerta-Lopez C, Velazquez-Carreras D, Viaris de Lesegno C, Ariotti N, Lazaro-Carrillo A, and Strippoli R (2019) An Abl-FBP17 mechanosensing system couples local plasma membrane curvature and stress fiber remodeling during mechanoadaptation. *Nat. Commun.* 10: 5828.

45. Takeuchi Y, Narumi R, Akiyama R, Vitiello E, Shirai T, Tanimura N, Kuromiya K, Ishikawa S, Kajita M, Tada M, and Haraoka Y (2020) Calcium wave promotes cell extrusion. *Curr. Biol.* 30: 670–681, e676.

46. Wu M, Wu X, and De Camilli P (2013) Calcium oscillations-coupled conversion of actin travelling waves to standing oscillations. *Proc. Natl. Acad. Sci. U. S. A.* 110: 1339–1344.